

The Laminar Burning Properties of Premixed Methane-Hydrogen Flames Determined Using a Novel Analysis Method

A.A. Burluka¹, M. Fairweather², M.P. Ormsby¹, C.G.W. Sheppard¹ and R. Woolley^{*1}

¹School of Mechanical Engineering, and ²School of Process, Environmental and Materials Engineering, University of Leeds, Leeds LS2 9JT, UK

Abstract

Laminar burning velocities, u_l , and Markstein lengths, L_b , have been obtained from spherically expanding flame experiments. A novel method, using least squares, of calculating u_l and L_b from the radius time record is presented. This avoids the amplification of noise in the experimental results when the radius time record is differentiated. Measurements were made for methane and methane/hydrogen mixtures (up to 50 % by volume hydrogen) with air at 0.1 MPa and 360 K. The addition of hydrogen resulted in increases in u_l , decreases in L_b (for constant equivalence ratio ϕ) and a widening of the ignition limits. Laminar burning velocities were also computed with a one dimensional solver for two published kinetic mechanisms.

Introduction

Hydrogen could be an important future energy carrier, offering CO₂ free emissions at the point of combustion. It has been proposed that existing natural gas pipelines could be employed for hydrogen transmission, with hydrogen mixed with natural gas. The mixture could then be used directly, or the hydrogen separated at the point of application (e.g. by differential diffusion using a suitable membrane) for use, for example, in engines or fuel cells. In the currently reported study experiments have been performed to determine burning rates to help quantify the risk resulting from accidental releases of natural gas-hydrogen mixtures

In these experiments pure methane was used to represent natural gas. A new and comprehensive data base on the burning velocity of hydrogen-methane mixtures has been generated. Data for premixed laminar flames at atmospheric pressure (0.1 MPa) for an initial temperature of 360 K are reported here (corresponding turbulent burning data are reported elsewhere [1]). Mixtures with air of pure methane (CH₄), 10, 20, and 50 % hydrogen in methane mixtures (referred to as 10 % H₂, 20 % H₂, 50 % hydrogen, respectively) were considered, with equivalence ratios ranging from lean ($\phi \leq 0.5$) to the rich ($\phi \geq 1.7$) ignition limits.

One-dimensional kinetic modelling of the laminar flames has also been performed, employing two published chemical kinetic models; GRI-Mech 3.0 [2] and Konnov [3]. Resultant laminar burning velocities are compared with experimentally derived data, and differences discussed below.

The laminar burning velocity of premixed fuel/air mixtures is now routinely obtained from spherically expanding flames captured using shadowgraphy or schlieren imaging [4, 5]. The flame radius may then be found by processing the resulting flame images and the

radius obtained directly from measurement of the flame area. In this way the unstretched flame speed, S_s , (and ultimately unstretched laminar burning velocity, u_l) and a Markstein length can be obtained [4]. The total stretch rate acting across the surface of a spherically expanding flame can be shown to be:

$$\alpha = \frac{2}{r_u} \frac{dr_u}{dt} = \frac{2}{r_u} S_n \quad (1)$$

where r_u is the flame radius. The burned gas Markstein length, L_b , is a proportionality coefficient between the local values of the observed stretched flame speed, S_n , and the stretch rate:

$$S_n = S_s - L_b \alpha \quad (2)$$

To derive L_b and S_s using Eq. (2) the radius-time record requires numerical differentiation. Such a procedure amplifies any noise, which is present when the radius is experimentally determined from the schlieren images.

After substitution of Eq. (1) into Eq. (2), rearrangement and integration with respect to time gives:

$$r_u(t) - r_u(t_0) + 2L_b \ln \left(\frac{r_u(t)}{r_u(t_0)} \right) = S_n(t - t_0). \quad (3)$$

Equation (3) is implicit for r_u but explicit for t . The resulting least squares function is:

$$\psi(L_b, S_n) = \sum_{i=1}^N \left(t_i - t_0 - \frac{r_i - r_0}{S_n} - 2 \frac{L_b}{S_n} \ln \frac{r_i}{r_0} \right)^2$$

and the conditions of its minimum

* Corresponding author: Rob.Woolley@sheffield.ac.uk
The University of Sheffield, Department of Mechanical Engineering, Mappin Street S1 3JD, UK
Proceedings of the European Combustion Meeting 2007

$$\frac{\partial \psi}{\partial S_n} = \frac{\partial \psi}{\partial L_b} = 0.$$

This results in

$$\sum_{i=1}^N \left(S_n (t_i - t_0) - (r_i - r_0) - 2L_b \ln \frac{r_i}{r_0} \right) \times \left(r_i - r_0 + 2L_b \ln \frac{r_i}{r_0} \right) = 0$$

$$\sum_{i=1}^N \left(S_n (t_i - t_0) - (r_i - r_0) - 2L_b \ln \frac{r_i}{r_0} \right) \ln \frac{r_i}{r_0} = 0$$

These two equations can be solved by multiplying by L_b and subtraction, giving:

$$S_n = \frac{c_1 b_{22} - c_2 b_{12}}{b_{11} b_{22} - b_{21} b_{12}}$$

$$L_b = \frac{c_2 b_{11} - c_1 b_{21}}{b_{11} b_{22} - b_{21} b_{12}}$$

where the coefficients are:

$$b_{11} = \sum (t_i - t_0)(r_i - r_0)$$

$$b_{12} = -2 \sum (r_i - r_0) \ln \frac{r_i}{r_0}$$

$$b_{21} = \sum (t_i - t_0) \ln \frac{r_i}{r_0}$$

$$b_{22} = -2 \sum \ln^2 \frac{r_i}{r_0}$$

$$c_1 = \sum (r_i - r_0)^2$$

$$c_2 = \sum (r_i - r_0) \ln \frac{r_i}{r_0}$$

In this way S_s and L_b can be solved without differentiating the radius-time measurements. Care must be taken with the selection of t_0 and r_0 . Simplistically one might assume that the flame has zero radius at time zero. However, the flame is initiated with a spark; resulting in more rapid growth in the early stages than might be the case if the growth rate was solely governed by Eq. (2). The influence of the spark on the initial flame growth was investigated in an earlier study [6] and found to be present up to a radius of 8 mm (for this ignition unit). Therefore determination of S_s and L_b was initiated from this point, with t_0 and r_0 adjusted accordingly.

Experimental

A 30 litre spherical stainless steel vessel was employed in the experiments. Three pairs of orthogonal quartz windows of diameter 150 mm provided excellent optical access. Turbulence was generated in the bomb

by four identical eight bladed fans, arranged in a tetrahedral configuration. In the ‘laminar’ experiments reported here the fans were stationary.

Mixture temperature was measured using a K type thermocouple, situated inside the chamber. The entire vessel was preheated by an internal 2 kW heater. A piezoresistive pressure transducer was employed to measure the pressure during mixture preparation. This transducer was situated outside the vessel and was isolated just prior to ignition.

Mixtures were prepared in the vessel, with gas concentrations set on the basis of partial pressures. After an experiment, the vessel was flushed with compressed air and then evacuated. Dry cylinder air was used in preparation of the combustible mixture. Fuel was supplied from high pressure cylinders containing set premixed hydrogen/methane mixtures (BOC). The fans were run during charge preparation to ensure full mixing and to maintain uniform heating of the vessel from the heater. The fans were switched off after the mixture was prepared, and the mixture left, for at least 60 seconds before ignition, allowing the mixture to become quiescent. An initial charge temperature of 360 K was adopted in all experiments, for convenience and compatibility with turbulent tests (not reported here). When the fans are run at high speed, kinetic heating would require vessel cooling for burning mixtures at room temperature. Estimated precision in the equivalence ratio setting was $\phi \pm 0.04$, a function of temperature variation during vessel filling and the accuracy of the pressure transducers.

Ignition was initiated from a purpose built stainless steel/ceramic sparkplug, with a gap of 1 mm, mounted in the centre of the vessel. A Lucas 12 V transistorised automotive ignition coil system was connected to the spark electrode assembly. The average spark energy was measured to be 23 mJ [7].

The flames were imaged using schlieren photography, employing of a 20 W tungsten element lamp, 1000 mm focal length lenses and a pinhole. The schlieren images were captured using a Photosonics Phantom 9 camera framing at 2000 fps. The resulting images were either hand traced or processed using Adobe PhotoShop 6.0. By subtracting the background (pre-explosion) image from the subsequent images and applying a threshold a binary image was produced for each frame where the burned area was white and the remainder black. The spark plug was manually removed. Flame areas were then measured by counting the number of pixels behind the flame front. Flame radii were computed as those of a circle of area equal to that of the imaged flame.

Flames ignited at the centre of the combustion vessel grew outward as essentially spherical flame balls. Typically, the flame surface were smooth, however, under certain circumstances, they spontaneously wrinkle and become ‘cellular’. Cellular flames were not observed in this study.

In the parallel modelling study, both chemical kinetic mechanisms examined were solved using

CHEMKIN PREMIX [8]. The GRI-Mech 3.0 consisted of 53 species, including NO_x chemistry [2]. The Konnov mechanism had 93 species, with NO_x chemistry removed [3], and generally took longer to compute a solution. The computations were run up to either a maximum of 200 grid points or GRAD and CURV to 0.1, whichever was achieved first.

Results and Discussion

Shown in Fig. 1 are flame radii plotted against time for three 50 % H₂ flames, at fuel-lean, stoichiometric and rich equivalence ratios. These flames were chosen as they should exhibit different responses to flame stretch, and hence have different Markstein lengths [4]. All three flames had very similar initial radii as the initial stages controlled by the same spark process. After ~ 2 ms, flame chemistry became dominant and differences between the three flames were immediately apparent. The rich flame slowed, and then started to accelerate again 10 ms after ignition. The lean and stoichiometric flames were faster than the rich flame, but their radii diverged as time increased due to a slight de-acceleration in the rich flame and acceleration in the stoichiometric flame.

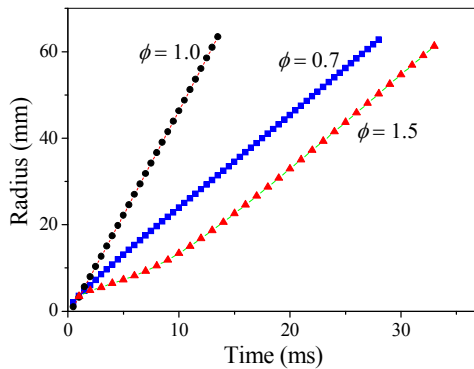


Fig. 1. Flame radius against time from ignition for 50% hydrogen flames at three equivalence ratios.

To demonstrate the determination of the laminar burning velocity and associated Markstein number, spherically expanding flames have been plotted on flame speed versus stretch graphs. These are shown for the three equivalence ratios in Figs. 2 – 4. The measured radii needed to be differentiated with respect to time to obtain the flame speed, this was performed using a three point central difference formula. Also shown are fits obtained using Eq. (2). The flames were processed in two ways: for Method 1 the least squares of the radius time data was adopted as detailed above; in Method 2 a linear least squares fit was performed on the differentiated flame speed / stretch curve [6]. For both methods only data from 8 mm onwards was included in the fit to ensure spark effects were removed.

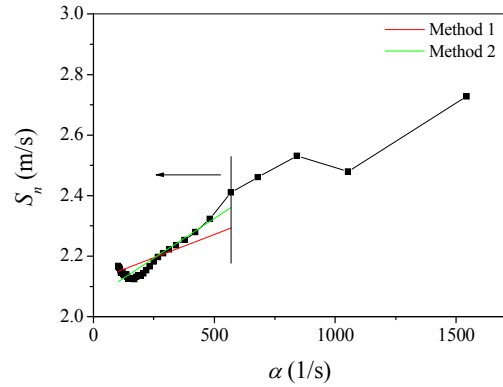


Fig. 2. Flame speed against stretch for a $\phi = 0.7$, 50% hydrogen/50% methane.

Data for the leanest mixture ($\phi = 0.7$) is shown in Fig. 2. The flame grows from right to left as flame stretch is inversely proportion to flame radius. The vertical line gives the assumed end of spark effects and the arrow shows the direction of increasing radius. As the flame grew its flame speed decreased by roughly 25%. Overall the experimental results are reasonably approximated by Eq. (2), despite a slight rise in the flame speed at large radii. The two methods give different fits resulting in different flame speeds and Markstein lengths, and these are given in Table 1. The cause in the rise in S_n at large radii is not known; simultaneous pressure measurements showed no significant increase, and no surface wrinkling was observed. Other flames did not show similar behaviour. Previous measurements of spherically expanding flames have had oscillations in the flame speed [6] and this could produce the observed rise, or it has also been shown that at low stretch rates the response of the flame speed can differ to that observed at higher stretch rates [9].

Shown in Fig. 3 are the results for a $\phi = 1.0$ flame. Here flame speed increases as stretch decreased, although by less than 5%. The higher flame speeds encountered resulted in measurements being performed over a much wider range of stretch rates compared with the $\phi = 0.7$ flame. The results for a rich flame ($\phi = 1.5$) are shown in Fig. 4, the flame responded very strongly to the decrease in the stretch rate, its flame speed doubling between 250 to 200 (1/s). The experimental data is poorly represented by Eq. (2). This more complicated behaviour, compared with the lean and stoichiometric flames, might be better fitted using a higher order equation requiring the adoption of at least 2 Markstein numbers [10].

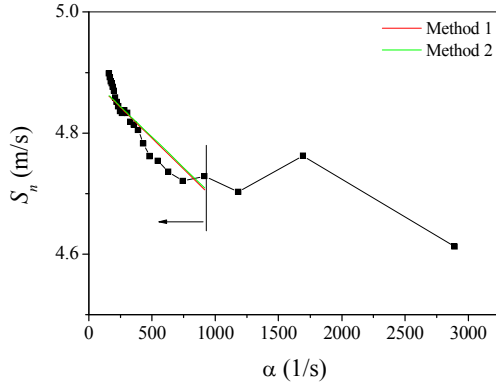


Fig. 3. Flame speed against stretch for a $\phi = 1.0$, 50% hydrogen/50% methane mixture.

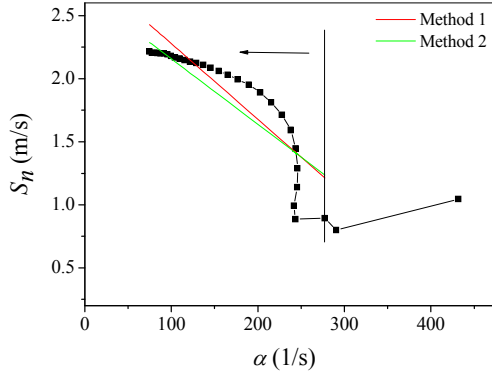


Fig. 4. Flame speed against stretch for a $\phi = 1.5$, 50% hydrogen/50% methane mixture.

ϕ	S_s (m/s)		L_b (mm)	
	1	2	1	2
0.7	2.12	2.06	-0.31	-0.52
1.0	4.89	4.89	0.20	0.20
1.5	2.88	2.68	6.01	5.20

Table 1. Unstretched flame speeds and Markstein Lengths.

Laminar burning velocities for all the fuels tested are shown in Fig. 5. The laminar burning velocity was obtained using the expression

$$u_l = \frac{\rho_b}{\rho_u} S_s \quad (4)$$

Where ρ_u and ρ_b are the unburned and burned gas densities. The addition of hydrogen generally increases u_l . For pure methane, flames could not be ignited beyond $\phi = 1.2$. However, the ignition limit was extended to $\phi = 1.4$ with the addition of only 10 % H_2 ,

and the rich ignition limit was extended to 1.6 for 50 % hydrogen. The addition of hydrogen did not have such a dramatic effect on the lean ignition limit, where the limit decreased from 0.6 to 0.5 (from pure methane to 10 % hydrogen), but did not change further as more H_2 was added. There was a noticeable shift in the peak burning velocity to richer ϕ with increasing hydrogen content. Although with 50% addition the peak which is around $\phi = 1.15$ is still significantly leaner than the peak for pure hydrogen which occurs at $\phi = 1.8$ [11].

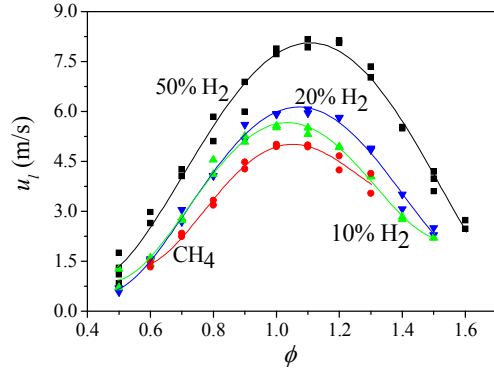


Fig. 5. Experimentally measured values of u_l against ϕ for all fuels, obtained using Method 2.

Values of L_b are shown in Fig. 6. All the fuels demonstrated a similar trend, an increase in L_b as ϕ increases. For each ϕ , methane had the highest L_b , which then dropped as hydrogen was added to the fuel. The 50 % H_2 could be approximated by $L_b \sim 0$ for $0.8 \leq \phi \leq 1.1$. For leaner (richer) mixtures L_b drops (rises) sharply. It has been shown that mixtures with lower Markstein lengths are likely to burn faster in turbulent flows especially at lean ϕ [12]. Therefore the 50 % H_2 fuel will burn faster in turbulent flows due to its higher laminar burning velocity and L_b .

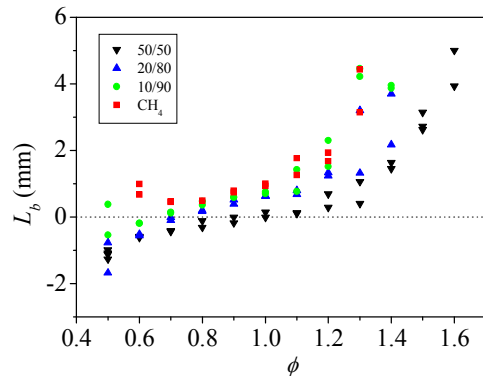


Fig. 6. Experimentally measured values of L_b against ϕ for all fuels, obtained using Method 2.

Comparisons between the experimentally derived values of u_l and those computed are shown in Fig. 7 for methane. Values determined using the GRI Mech proved consistently higher than those of Konnov. This is likely to reflect the experimental data used to

'calibrate' the mechanism, as GRI used data primarily from counterflow burners [13]. This experimental configuration tends to give consistently (slightly) higher u_l 's those obtained using spherically expanding flames [14]. The Konnov mechanism, compiled slightly later (when more experimentally determined laminar burning velocities were available) yielded slightly lower values of u_l . The experimental results sit between the two, except at the extremes in ϕ . For lean mixtures the Konnov mechanism matches the experiments closely. At rich ϕ the assumption of a single L_b has been demonstrated to be questionable. That the experimental u_l were higher than both the modelled results might support fitting at lower values of α (larger radii).

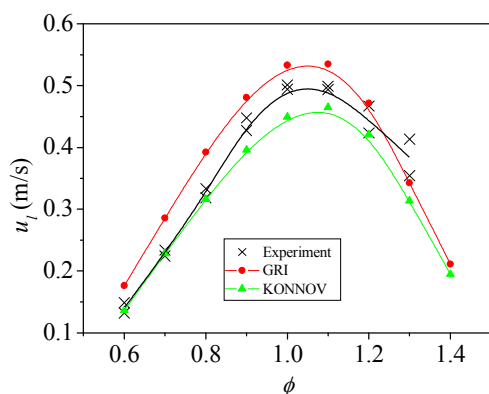


Fig. 7. Comparison of experimental and modelled values of u_l for CH_4 .

Model and experimentally determined u_l 's are compared in Fig. 8 for 50 % H_2 . Here, the agreement between the experiments and the Konnov mechanism can be seen to be very close, with those yielded by GRI Mech again consistently higher than the data.

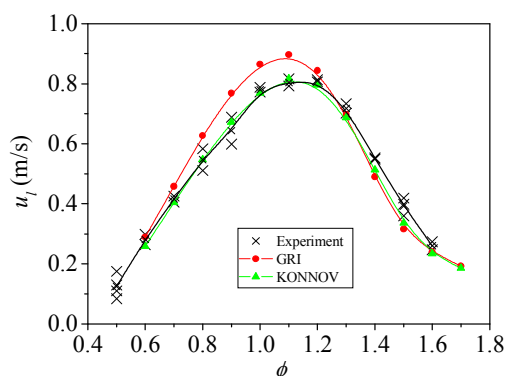


Fig. 8. Comparison of experimental and modelled values of u_l for 50 % H_2 .

Conclusions

A method, using least squares, of calculating the laminar burning velocity and Markstein length from the radius time record of a spherically expanding laminar flame has been presented.

The influence of processing methods has been compared and the differences found to depend on the equivalence ratio (or stretch response) of the flame.

The addition of hydrogen to methane resulted in an increase in measured laminar burning velocity and decrease in Markstein length. It also increased the ignition limits, particularly at fuel-rich equivalence ratios.

Comparisons were made between experimental data and one-dimensional kinetic computations for u_l , using two full chemistry mechanisms, with reasonable agreement with data found. Overall the more recently constructed scheme by Konnov performed best, although this is likely to be a result of the more extensive experimental database used for its validation.

Acknowledgements

The authors gratefully acknowledge financial support from the EC's 6th Framework Programme (Integrated Project NATURALHY – SES6/CT/2004/50266).

References

- [1] M. Fairweather, M.P. Ormsby, C.G.W. Sheppard, R. Woolley, Turbulent burning rates of hydrogen methane mixtures (in preparation).
- [2] P.G. Smith, D.M. Golden, M. Frenklach, N.W. Moriarty, M. Goldenberg, C.T. Bowman, R.K. Hanson, S. Song, W.C. Gardiner Jr., V.V. Lissianski, Z. Oin, from http://www.me.berkeley.edu/gri_mech/
- [3] A. Konnov, from <http://homepages.vub.ac.be/~akonnov/>
- [4] X.J. Gu, M.Z. Haq, M. Lawes, R. Woolley, *Combust. Flame* 121 (2000) 41-58.
- [5] M.I. Hassan, K.T. Aung, G.M. Faeth, *Combust. Flame* 115 (1998) 539-550.
- [6] D. Bradley, R.A. Hicks, M. Lawes, C.G.W. Sheppard, R. Woolley, *Combust. Flame* 115 (1998) 126-144.
- [7] D. Bradley, R.A. Hicks, M. Lawes, C.G.W. Sheppard. Technical Report, Department of Mechanical Engineering, The University of Leeds, UK (1996).
- [8] R.J. Kee, J.F. Grgar, M.D. Smooke, J.A. Miller, A Fortran Program for Modeling Steady Laminar One-Dimensional Premixed Flames, Report No. SAND85-8240, Sandia National Laboratories, 1985.
- [9] J.A.M. de Swart, G.R.A. Groot, J.A. van Oijena, J.H.M. ten Thije Boonkamp, L.P.H. de Goey, *Combust. Flame* 145 (2006) 245-258.
- [10] Clavin, P., *Prog. Energy Combust. Sci.* 11 (1985) 1-59.
- [11] D.R. Dowdy, D.B. Smith, S.C. Taylor, A. Williams, *Proc. Combust. Inst.* 23 (1991) 325-332.
- [12] A.N. Lipatnikov, J. Chomiak, *Prog. Energy Combust. Sci.* 31 (2005) 1-73.
- [13] Egolfopoulos, F.N., Cho, P., and Law, C.K., *Combust. Flame* 76 (1989) 375-391.
- [14] Taylor, S.C. (1991). Ph.D. dissertation, The University of Leeds, Department of Fuel and Energy.